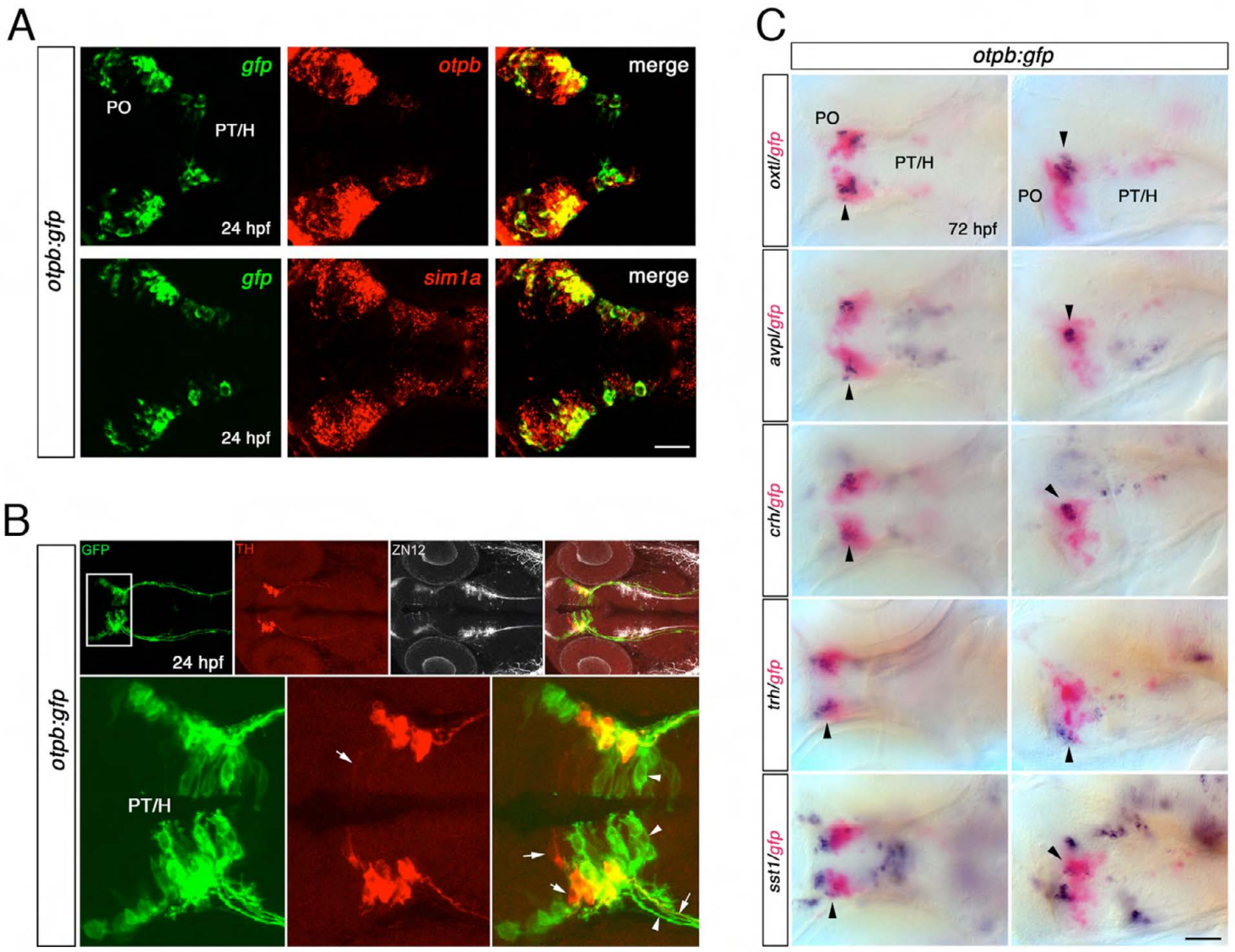

Fig. S1. The *otpb:gfp* reporter line recapitulates many aspects of endogenous *otpb* expression in the forebrain. (**A**) Dorsal views of confocal *z* projections of the forebrain region of *otpb:gfp* transgenic embryos at 24 hpf, demonstrating co-expression of *gfp* (green) and *otpb* (red), as well as co-expression of *gfp* (green) and *sim1a* (red) analyzed by double fluorescent in situ hybridization are shown. Scale bar: 50 μm. (**B**) Dorsal views of *otpb:gfp* transgenic embryos at 24 hpf co-labeled with anti-GFP (green), anti-TH (red) and anti-ZN12. Dopaminergic TH-positive cell bodies and longitudinal dopaminergic projections are immunoreactive for GFP (arrows). Scale bar: 100 μm. (**C**) Dorsal (left panel) and lateral views (right panel) of *otpb:gfp* transgenic embryos at 72 hpf analyzed for co-expression of hypothalamic neurohormones (shown in blue) and *gfp* (shown in purple) by double in situ hybridization. Oxytocin-like (*oxtl*), arginine vasopressin-like (*avpl*), corticotropin releasing hormone (*crh*), thyrotropin releasing hormone (*trh*) and somatostatin 1 (*sst1*) transcripts in the preoptic region all colocalize with *gfp* expression (see arrowheads). Scale bar: 50 μm. PT, posterior tuberculum; H, hypothalamus; PO, preoptic region.

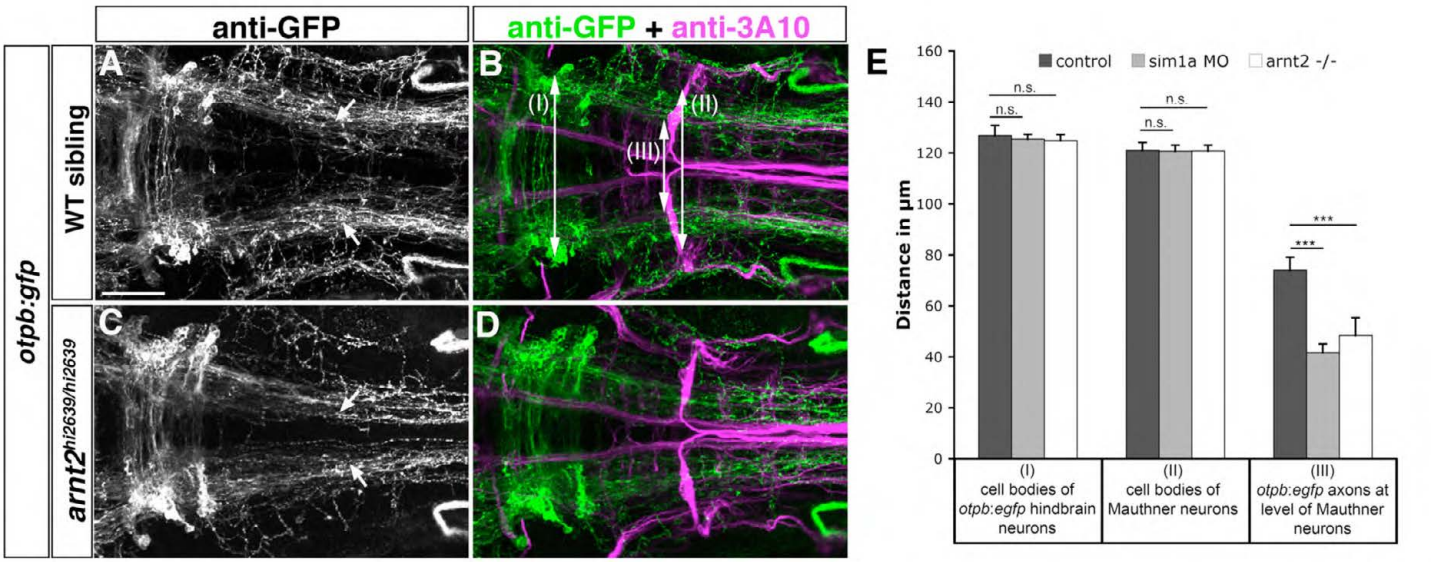

Fig. S2. Lateral positioning of longitudinal *otpb:gfp*-positive axons is altered in *arnt2*^{hi2639c} mutants. Dorsal views of confocal *z* projections of the hindbrain of *otpb:gfp* transgenic embryos co-labeled with anti-GFP and anti-3A10 (A-D) at 72 hpf are shown. (**A**,**B**) Wild-type siblings display normal medio-lateral positioning of *otpb:gfp* positive axons (arrows in A). (**C**,**D**) In *arnt2*$^{hi2639c/hi2639c}$ homozygous mutants, longitudinal projections of *otpb:gfp* axons are shifted towards the midline (arrows in C). Midline crossing of Mauthner axons is not affected in *arnt2*^{hi2639c} mutants, suggesting grossly normal hindbrain development (compare arrowheads in B,D). (**E**) Quantification of mediolateral positioning of *otpb:gfp*-positive longitudinal axons at the anterior-posterior level of Mauthner neurons (see III in B), of the distance of MA neurons (see II in B) and of *otpb:gfp* hindbrain neurons (see I in B) in *arnt2*$^{hi2639c/hi2639c}$ homozygous mutants or wild-type siblings. Numbers in parentheses indicate the number of embryos analyzed. ***P<0.0001; n.s., not significant. Scale bar: 50 µm.

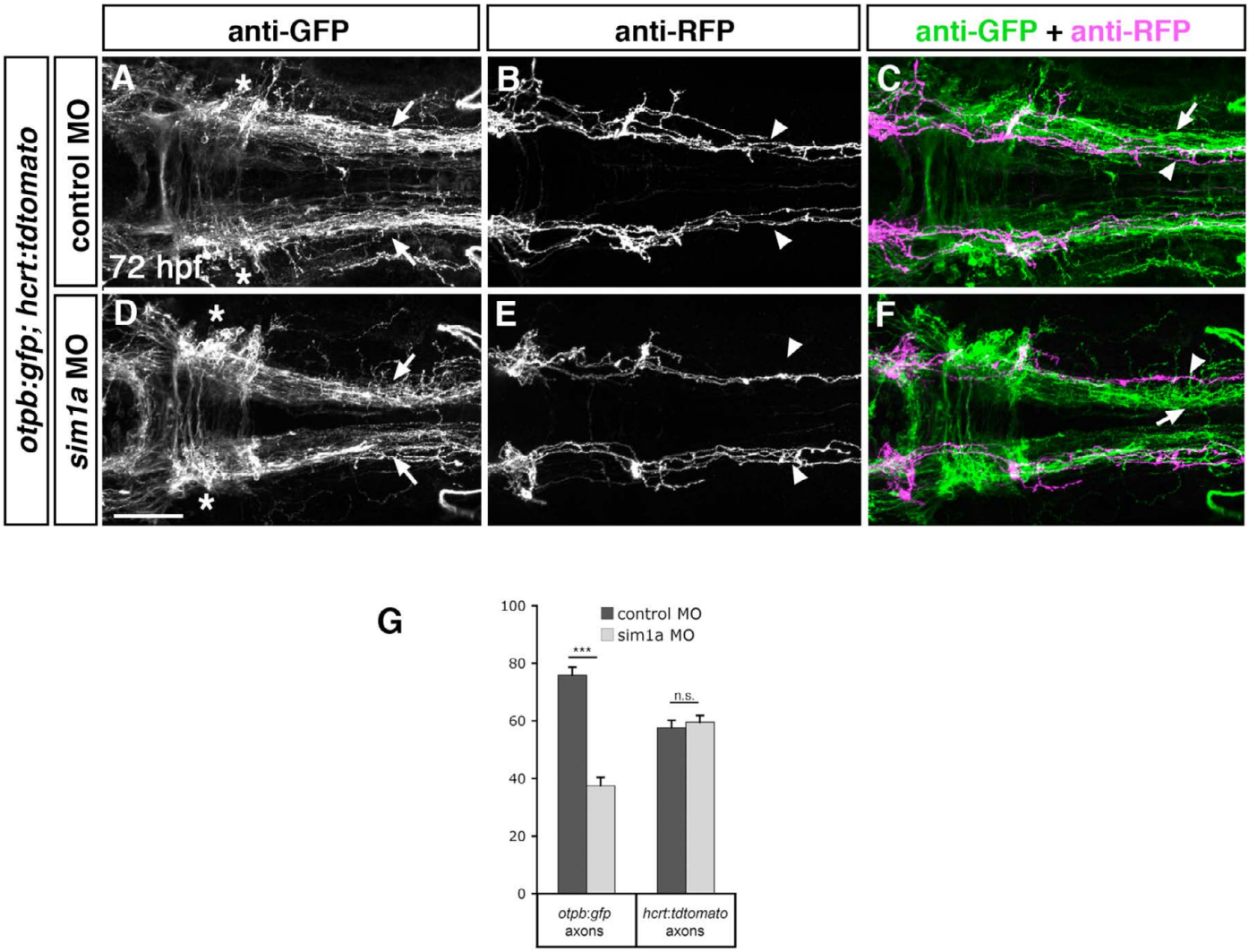

Fig. S3. Loss of Sim1a function causes medial displacement of longitudinal *otpb:gfp*-positive axons. Dorsal views of hindbrain confocal *z* projections of *otpb:gfp;hcrt:tdtomato* double transgenic embryos at 72 hpf. (**A-F**) *otpb:gfp* axons (arrows in D,F) in *sim1a* morphants display strong medial displacement compared with controls (A,C) *hcrt:tdtomato* axons (arrowheads in B,C,E,F) are not affected. *otpb:gfp* hindbrain neurons (asterisks in A,D) do not contribute to longitudinal projections. (**G**) Quantification of mediolateral positioning of *otpb:gfp* and *hcrt:tdtomato* axons at the level of Mauthner neurons at 72 hpf after control or *sim1a* MO injection. ***$P<0.0001$; n.s., not significant. Scale bar: 50 μm for A-F.

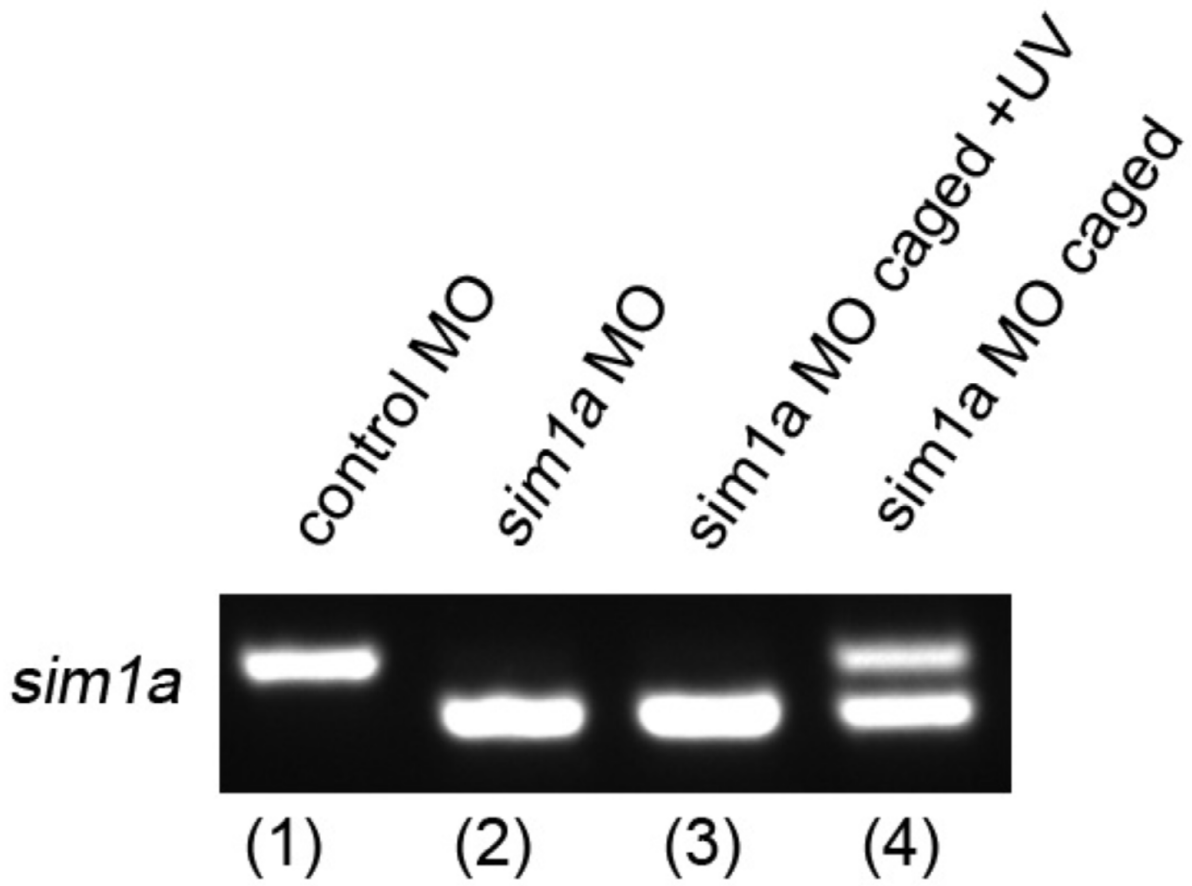

Fig. S4. Temporal control of *sim1a* knockdown using photomorph technology. RT-PCR demonstrating efficacy of temporal control of *sim1a* knockdown. Lane 1, 4.5 ng standard control MO; lane 2, 1 ng *sim1a* MO; lane 3, 1 ng caged *sim1a* MO (=photomorph), which was photocleaved by UV light; lane 4, 1 ng caged *sim1a* MO without UV cleavage. The upper band represents wild-type *sim1a* transcript, the lower band represents the morphant transcript eliminating exon 2. The caging strand never fully blocked the morpholino but instead caused a partial *sim1a* knockdown with residual wild-type transcript. Pooled cDNAs from five injected embryos of each condition were used for analysis.

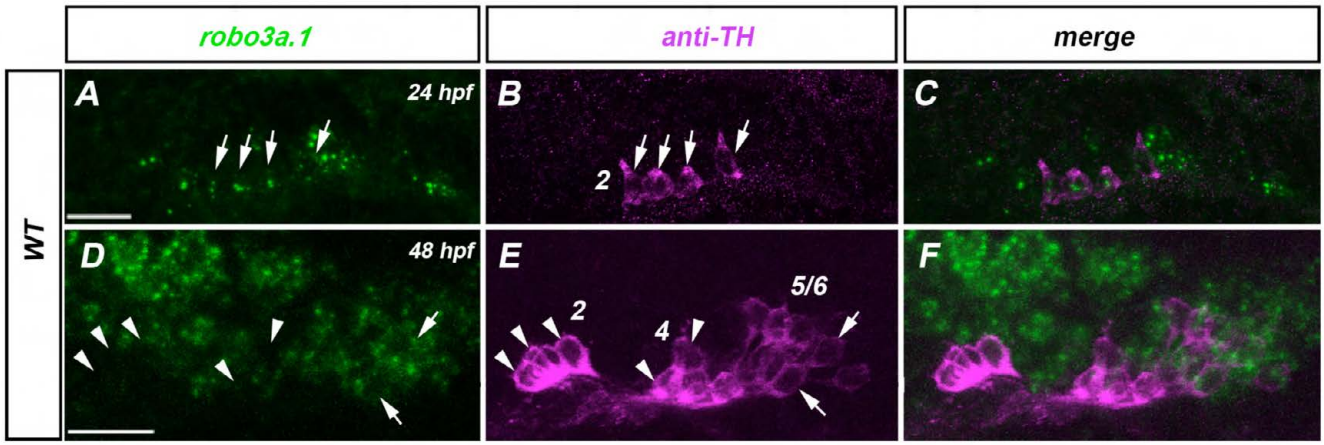

Fig. S5. Expression of *robo3a.1* during development of hypothalamic DA neurons. Dorsal views of confocal *z* projections at the anterior-posterior level of the hypothalamus at indicated developmental stages. Anterior is towards the left. Only the left side of the brain is depicted. (**A-C**) At 24 hpf, expression of *robo3a.1* is found in group 2 TH-positive DA neurons (see arrows in A,B). (**D-F**) At 48 hpf, expression of *robo3a.1* in group 2 and group 4 TH-positive DA neurons is almost undetectable (arrowheads in D-E), whereas group 5-6 TH-positive DA neurons express *robo3a.1*. Numbers in B and E indicate DA neuronal groups according to Rink and Wullimann (Rink and Wullimann, 2002). Scale bars: 25 μm.

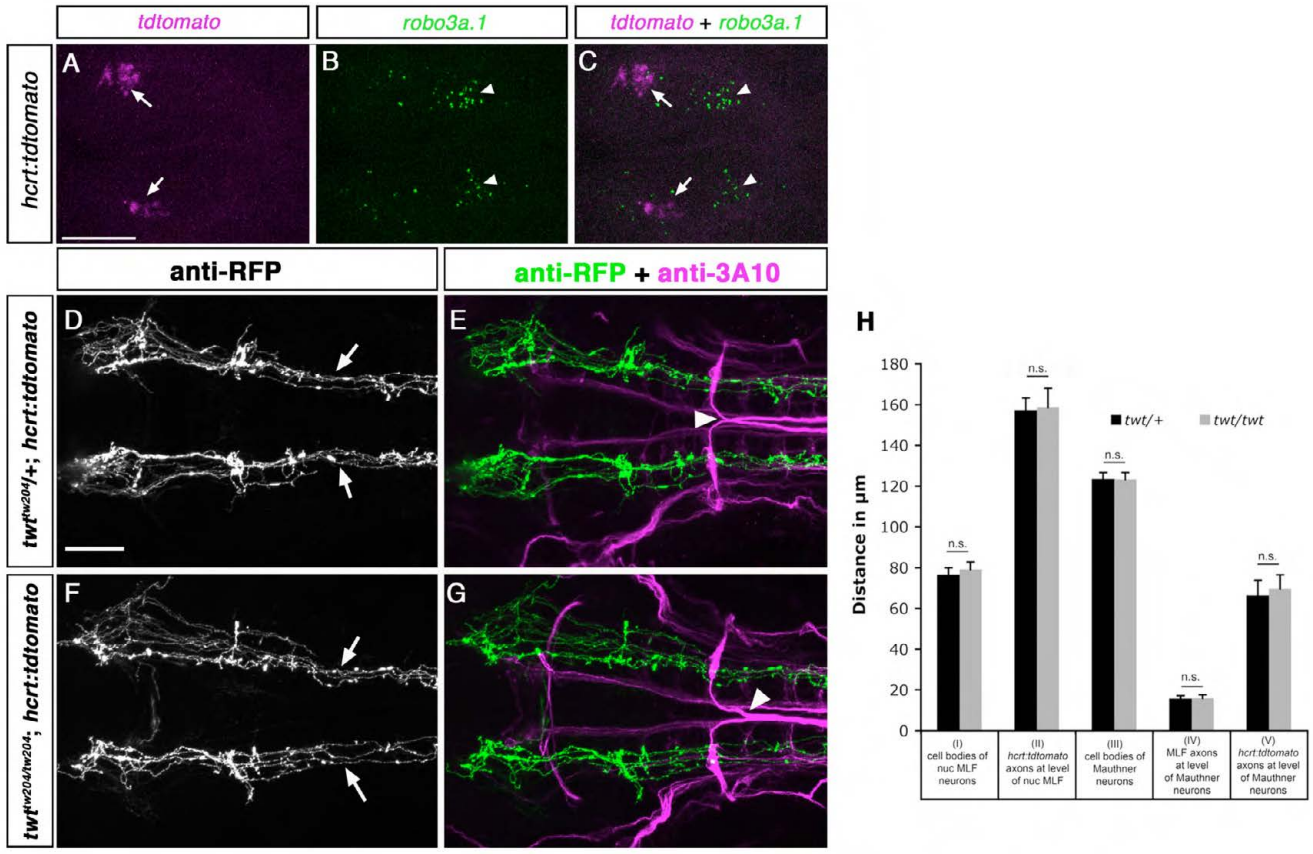

Fig. S6. *robo3* is not required for HTS longitudinal tract formation of Hcrt neurons. Dorsal views of confocal *z* projections of the brain of 24 hpf embryos (A-C) or hindbrain of 72 hpf embryos are shown. Anterior is towards the left. (**A-C**) Whole-mount fluorescent *in situ* hybridization for *tdtomato* and *robo3a.1* expression in *hcrt:tdtomato* embryos are shown. *robo3a.1* (arrowheads in B,C) was not detectable in Hcrt neurons (arrows in A,C). (**D-G**) Immunohistochemistry with anti-RFP and anti-3A10 antibodies demonstrates that pathfinding of TdTomato-positive longitudinal axons is similar in *twt*^{tw204}/+;*hcrt:tdtomato* (arrows in D) when compared with *twt*$^{tw204/tw204}$;*hcrt:tdtomato* embryos (arrows in F). Arrowheads in E indicate normal midline crossing of Mauthner axons in heterozygous *robo3* embryos; arrowhead in G denotes abnormal crossing of Mauthner axons in homozygous *robo3* mutants. (**H**) Quantification of the distance between nucMLF neurons (I) and MLF axons (III), *hcrt:tdtomato* longitudinal axons at two different positions (II +IV) and MA neurons (V) in *twt*/+ and *twt*/*twt* embryos. n.s., not significant. Scale bars: in A, 50 μm for A-C; in D, 50 μm for D-G.

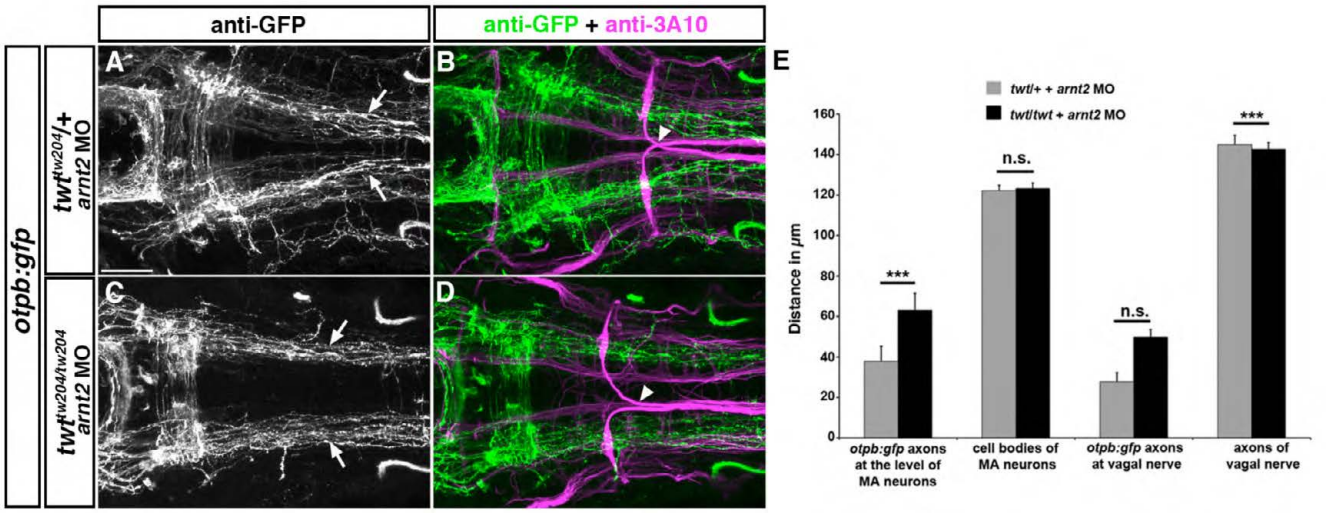

Fig. S7. Medial displacement of *otpb:gfp*-positive longitudinal axons is reduced in *robo3* mutants after *arnt2* knockdown. Dorsal views of *z* projections of the hindbrain of 72 hpf embryos labeled with anti-GFP and anti-3A10 antibodies are shown. Anterior is towards the left. (**A**,**B**) In twt^{tw204}/+;*otpb:gfp* embryos injected with *arnt2* MO *otpb:gfp*-positive longitudinal axons (arrows in A) grow towards the midline. Midline crossing of Mauthner axons is normal (arrowhead in B). (**C**,**D**) After knock down of *arnt2* in $twt^{tw204/tw204}$;*otpb:gfp* embryos, longitudinal axons project in a wild-type manner (arrows in C). Abnormal crossing of Mauthner axons (arrowhead in D) indicates homozygous *robo3* mutant. (**E**) Quantification of the distance of MA neurons and of medio-lateral positioning of *otpb:gfp*-positive longitudinal axons at the anterior-posterior level of Mauthner neurons and medio-lateral positioning of *otpb:gfp* vagal axons. **P*<0.001, Student's *t*-test; n.s., not significant). Scale bar: 50 µm.

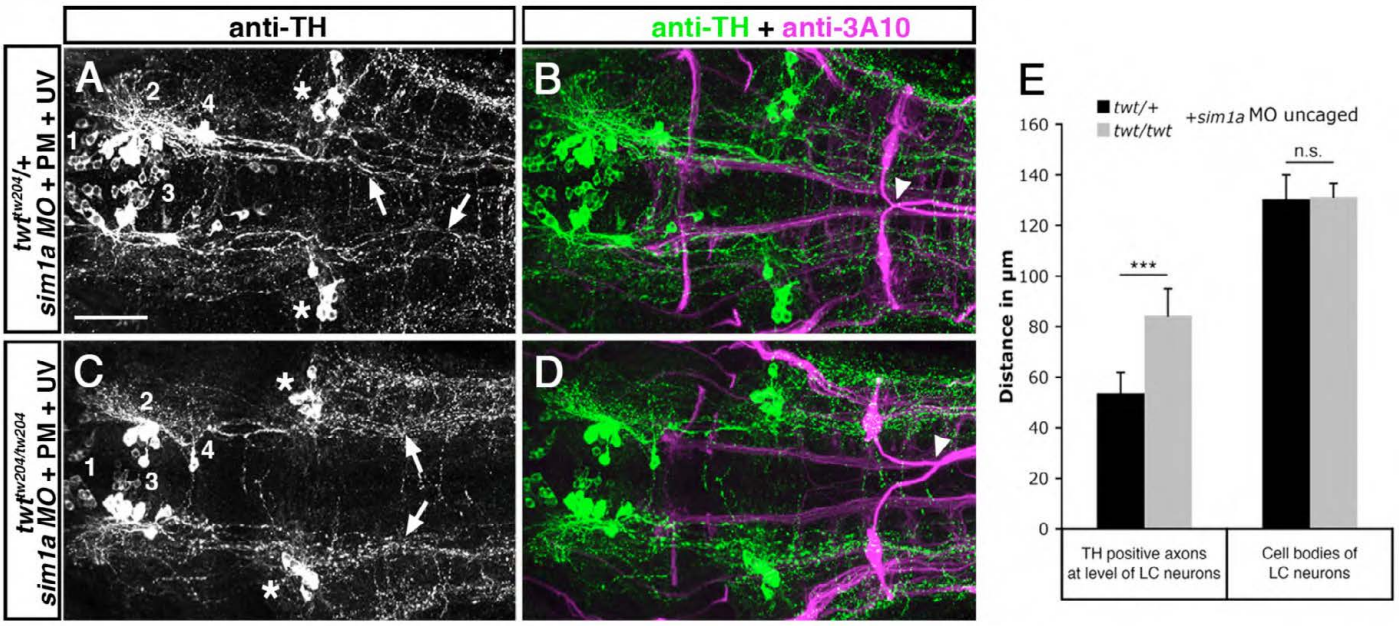

Fig. S8. Medial displacement of TH-positive longitudinal axons in *robo3* mutants is reduced after temporally controlled *sim1a* knockdown. Dorsal views of confocal *z* projections of the hindbrain of 72 hpf embryos labeled with anti-TH and anti-3A10 antibodies are shown. (**A**,**B**) Longitudinal TH-positive axons derived from group 2 and 4 DA neurons are shifted towards the midline (arrows in A) after photoactivation of *sim1a* MO at 22 hpf in twt^{tw204}/+ embryos. Midline crossing of Mauthner axons is normal (arrowhead in B). (**C**,**D**) After temporally controlled activation of *sim1a* MO in $twt^{tw204/tw204}$ embryos at 22 hpf, TH-positive longitudinal axons derived from group 2 and 4 DA neurons project in a wild-type-like fashion (arrows in C). Abnormal crossing of Mauthner axons (arrowhead in D) indicates homozygous *robo3* mutant. (**E**) Quantification of medio-lateral positioning of TH-positive longitudinal axons in $twt^{tw204/+}$ and $twt^{tw204/tw204}$ embryos after temporally controlled activation of *sim1a* MO. Asterisks in A and C indicate noradrenergic locus coeruleus neurons. PM, photomorph; UV, ultra violet. Numbers in A and C indicate DA neuronal groups according to nomenclature of Rink and Wullimann (Rink and Wullimann, 2002). **P*< 0.001, Student's *t*-test; n.s., not significant. Scale bar: 50 µm for A-D.

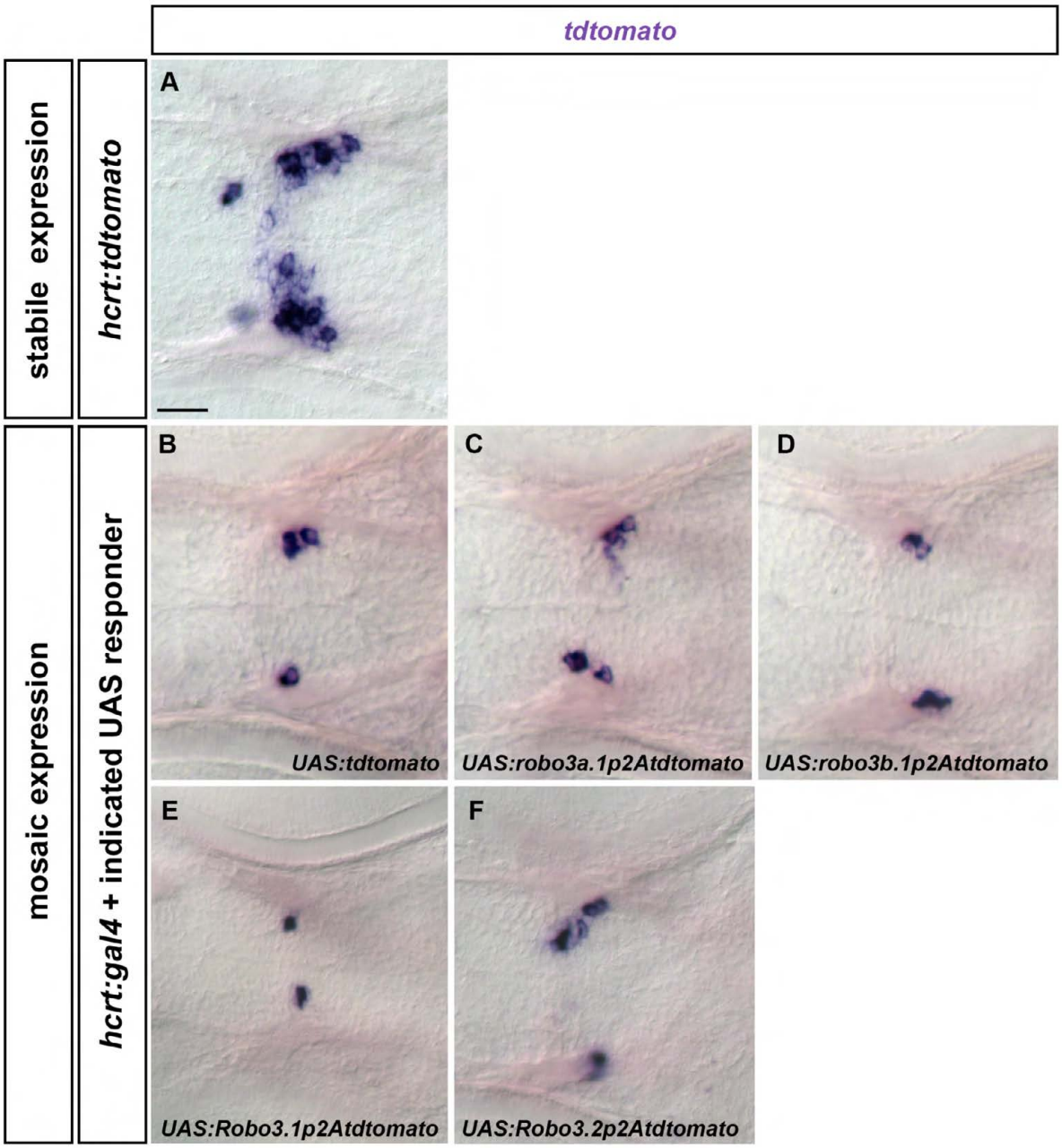

Fig. S9. Expression of *tdtomato* derived from different UAS constructs co-injected with *hcrt:gal4.* Whole-mount *in situ* hybridization showing *tdtomato* expression. Dorsal views of the brain of 72 hpf embryos are shown. Anterior is leftwards. (**A**) Expression of *tdtomato* in a stabile *hcrt:tdtomato* transgenic embryo is shown to illustrate localization of *hcrt* neurons. (**B-F**) Similar levels of transient *tdtomato* expression can be detected after combined injection of *hcrt:gal4* and the indicated UAS constructs. Developing time of the *in situ* hybridization signal for embryos shown in B-D or in E,F was equal. Scale bar: 25 μm.

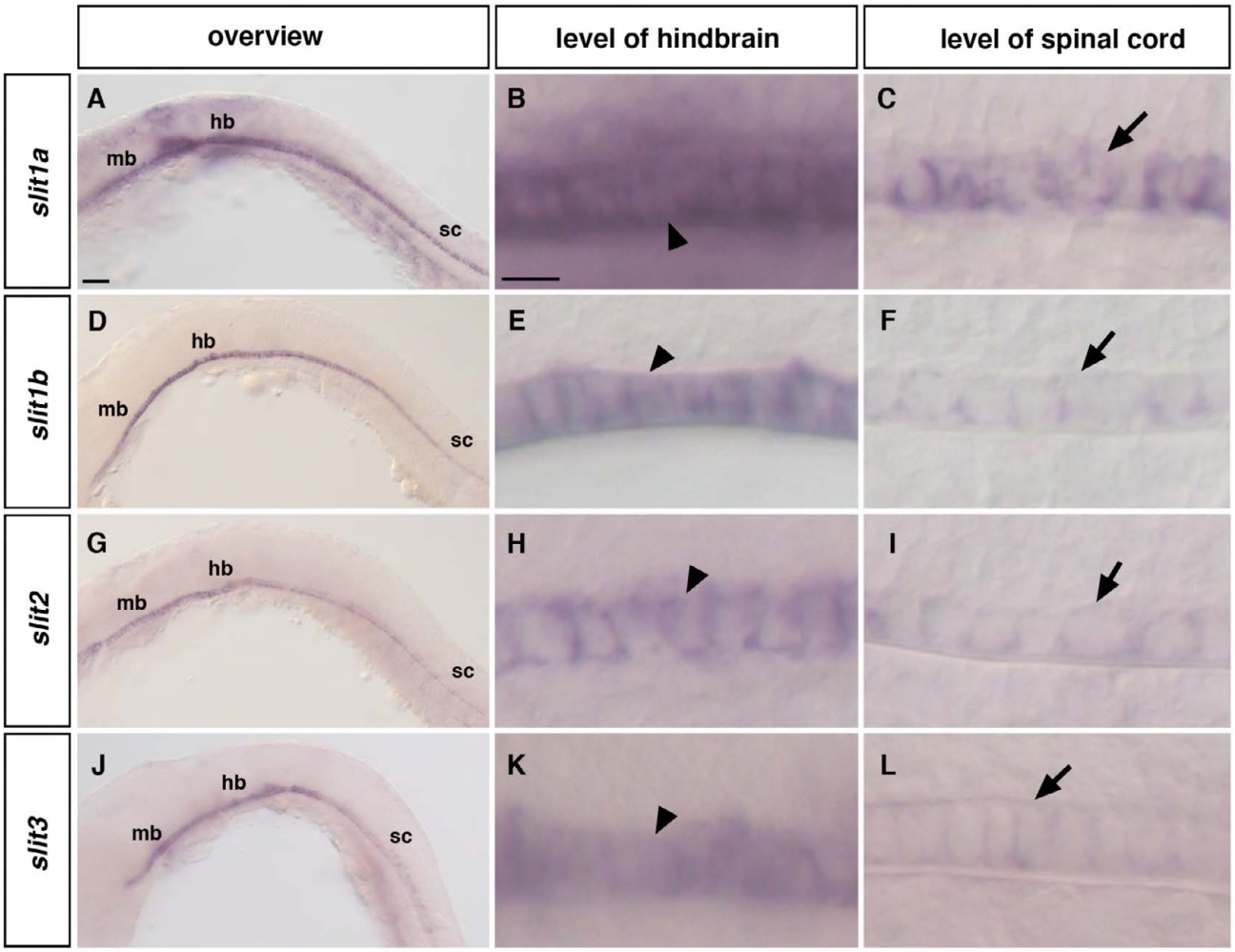

Fig. S10. *slit1*, *slit1b*, *slit2* and *slit3 in situ* hybridization at 24 hpf. Whole-mount in situ hybridization showing *slit1a* (A-C), *slit1b* (D,E), *slit2* (G-I) and *slit3* (J-L) expression. Lateral views of 24 hpf embryos (A,D,G,J), of the floor plate at the level of the hindbrain (B,E,H,K), and of the floor plate at the level of the spinal cord (C,F,I,L) are shown. Anterior to left. (**A-L**) Strong expression of the four different *slit* genes was found in midbrain and hindbrain regions when compared with spinal cord. Higher magnification revealed strong expression of the different slit genes within the floor plate at the level of the hindbrain (arrowheads in B,E,H,K) when compared with floor-plate cells at the level of the spinal cord (arrows in C,F,I,L) mb, midbrain; hb, hindbrain; sc, spinal cord. hb and sc labels also indicate the position of the floor-plate regions shown in higher magnification. Scale bars: in A, 100 μm for A,D,G,J; in B, 50 μm for B,C,E,F,H,I,K,L.

Table S1. Zebrafish mutant/transgenic lines used in this study

Genotype	Reference
arnt2^{hi2639}	Golling et al., 2002
astray (ast^{ti272z}*)*	Fricke et al., 2001
astray (ast^{te284}*)*	Fricke et al., 2001
twitch twice (twt^{tw204}*)*	Burgess et al., 2009
hcrt:tdtomato^{m1163}	This study
hsp70l:robo3b.1iresegfp^{m1217} a.k.a. *hsp70l:robo3b.1*	This study
hsp70l:robo3a.1iresegfp^{m1218} a.k.a *hsp70l:robo3a.1*	This study
Tg*(otpb:1EGFP)*^{zc49} a.k.a *otpb:egfp*	Fujimoto et al., 2011

Table S2. Antibodies and probes

Primary and secondary antibodies for immunohistochemistry	
Anti-Tyrosine Hydroxylase (1:500)	Ryu et al., 2007
Anti-3A10 (1:50)	Furley et al., 1990, Developmental Studies Hybridoma Bank, University of Iowa
Anti-GFP (1:400)	Molecular Probes
Anti-GFP (1:500)	(clone JL-8, Clontech)
Anti-RFP/DsRed/TdTomato (1:500)	MBL
Secondary antibodies were coupled to Alexa-488, Alexa-555 or Alexa-633 (Invitrogen), all used 1:1000.	
List of probes for *in situ* hybridization	
Digoxigenin (Roche), Fluorescein (Roche) or DNP (Molecular Probes) labelled probes were prepared for the following genes: *robo2*, *robo3b.1*, *robo3a.1*, *otpb*, *sim1a*, *oxtl*, *avpl*, *crh*, *trh*, *sst1, slit1a, slit1b, slit2, slit3* and *dcc* (for references see: www.zfin.org). For *gfp* and *tdtomato* probes, partial *gfp* or *tdtomato* coding sequence was subcloned into pCRII-TOPO vector (Invitrogen).	

Table S3. Entry vectors used for multisite gateway system and of complete expression vectors

Vectors	Cloning
p5E-hypocretin	A fragment containing 1 kb hypocretin promoter (Faraco et al., 2006) was subcloned into p5E-MCS.
pME-*robo3b.1* and pME-*robo3a.1*	Full length coding sequences of *robo3* variant 1 (*robo3b.1*) and variant 2 (*robo3a.1*) were amplified from adult brain cDNA and subcloned into pCRII-TOPO (Invitrogen). (robo3b.1_f: 5'- ATGGAGTTTCGCAGGACTTT -3'; robo3a.1_f 5'-ATGCTGCGTTACCTGATAAAGAC-3'; robo3_common_r 5'-TTATCTCATCTCATCATTTCTCTTCCT -3'). Gateway compatible attB1 and attB2 sites were added by PCR. Derived PCR products were recombined into pDONR221 to yield *pME-robo3a.1* and *pME-robo3b.1*.
pME-*Robo3A.1 and* pME-*Robo3A.2*	The mouse *Robo3A.1* and *Robo3A.2* coding sequences were amplified from pCAGGS-*Robo3A.1-myc* or pCAGGS-*Robo3A.2-myc* (Chen et al., 2008) using Gateway-compatible primers. The PCR fragments were subsequently recombined into pDONR221 vector to yield pME-*robo3b.1*, pME-*robo3a.1*, *pME-Robo3A.1* and *pME-Robo3A.2*
pME-tdTomatoCAAX	attB1/B2 sites and a membrane tag encoding the CAAX box of human Harvey Ras (5'-AAGCTGAACCCTCCTGATGAGAGTGGCCCCGGCTGCATGAGCTGCAAGTGTGTGCT CTCCTGA-3') were attached to full length tandemTomato coding sequence (ptdTomatoN1, Clontech) via PCR using Gateway-compatible primers. Derived PCR product was recombined into pDONR221 to yield pME-tdTomatoCAAX.
p3E-P2A-tdTomatoCAAX	att B2r/B3 sites as well as viral P2A (Holst et al., 2006) and human Harvey Ras CAAX cassettes were attached to full length tandemTomato coding sequence via PCR amplification using Gateway-compatible primers and recombined into pDONRP2R-P3 to yield *p3E-P2A-tdTomatoCAAX.*

Subsequent multisite gateway recombination (LR reactions) yielded the desired expression constructs listed below

Cloned expression constructs for transient analyses or generation of stable lines
pDestTol2pA2;hcrt:tdTomatoCAAX-pA
pDestTol2CG2;hcrt:Gal4VP16-pA
pDestTol2CG2;hsp70l:robo3a.1-IRES-EGFP
pDestTol2CG2;hsp70l:robo3b.1-IRES-EGFP
pDestTol2CG2;UAS:robo3a.1-P2A-tdTomatoCAAX
pDestTol2CG2;UAS:Robo3A.1-P2A-tdTomatoCAAX
pDestTol2CG2;UAS:Robo3A.2-P2A-tdTomatoCAAX
pDestTol2CG2;UAS:robo3b.1-P2A-tdTomatoCAAX
pDestTol2CG2;UAS:tdTomatoCAAX-pA

Table S4. Quantification of axon guidance defects after knock down of *sim1a* or *arnt2* (Fig.1 and Fig.S2/S3).

Genotype	***n***	**Injection**	**Average distance between *otpb:gfp longitudinal* axons at the level of the MA neurons**	**Average distance between *hcrt:tdtomato* longitudinal axons at the level of the MA neurons**	**Average distance between MA neurons**
otpb:gfp;hcrt:tdtomato	7	*control* MO (1ng)	75.9 ± 2.7 µm	57.6 ± 2.9 µm	124.2 ± 2.5
otpb:gfp;hcrt:tdtomato	7	*sim1a* MO (1ng)	47.1 ± 5.9 µm	59.5 ± 2.3 µm	122.8 ± 2.6

Genotype	***n***	**Injection**	**Average distance between *otpb:gfp* longitudinal axons at the level of the MA neurons**	**Average distance between MA neurons**
otpb:gfp	14	control MO (4.5 ng)	69.7 ± 7.3 µm	124.1 ± 1.7
otpb:gfp	14	*sim1a* MO (1 ng)	42.6 ± 3.9 µm	123.3 ± 2.6
otpb:gfp	16	*sim1a* MO (0.25 ng)	69.4 ± 3.4 µm	125.2 ± 2.3
arnt2^{hi2639c}, otpb:gfp	9		48.4 ± 6.9 µm	124.2 ± 3.9
otpb:gfp	13	*arnt2* MO (4.5 ng)	44.5 ± 5.6 µm	124.7 ± 2.6 µm
otpb:gfp	15	*arnt2* MO (1 ng)	67.3 ± 2.6 µm	124.3 ± 1.7 µm
otpb:gfp	16	*arnt2* MO (1 ng) + *sim1a* MO (0.25 ng)	42.5 ± 8.2 µm	123.1 ± 2.5 µm

Genotype	***n***	**Injection**	**Average distance between *otpb:gfp* neurons in hindbrain**
otpb:gfp	14	control MO	126.3 ± 3.8 µm
otpb:gfp	14	*sim1a* MO	125.5 ± 1.7 µm
otpb:gfp	16	*sim1a* MO (0.25 ng)	124.8 ± 3.2 µm
arnt2^{hi2639c}, otpb:gfp	9		124.4 ± 2.8 µm
otpb:gfp	13	*arnt2* MO (4.5 ng)	125.6 ± 2.6 µm
otpb:gfp	15	*arnt2* MO (1 ng)	124.4 ± 2.7 µm
otpb:gfp	16	*arnt2* MO (1 ng) + *sim1a* MO (0.25 ng)	124.3 ± 3.4 µm

To quantify the axon guidance phenotypes upon depletion of *sim1a* or *arnt2*, we determined the distance between the *otpb:gfp* or *hcrt:tdtomato* longitudinal axons at the level of the Mauthner neurons (Fig. S2B). To control for the specificity of the observed effects, we measured the distance between the MA neurons and between the *otpb:gfp* neurons in the hindbrain (Fig. S2B). For *otpb:gfp* longitudinal axons. This analysis revealed a significant difference in the distance of longitudinal *otpb:gfp* axons upon injection of 1 ng *sim1a* MO, 4.5 ng *arnt2* MO or in *arnt2^{hi2639c}* mutants when compared with 0.25 ng *sim1a* MO-, 1 ng *arnt2* MO- or 4.5 ng control MO-injected embryos. The amount of injected MO is indicated as ng/embryo. The distance between longitudinal *hcrt:tdtomato* axons, MA neurons or hindbrain *otpb:gfp* neurons was not different.

Table S5. Quantifications of HTS axon guidance defects observed in *sim1a* photomorph experiment (see Fig. 2)

Genotype	***n***	**Injection**	**Average distance between longitudinal TH positive axons at the level of the LC neurons**	**Average distance between LC neurons**
otpb:gfp	13	*sim1a + PM + UV*	54.1 ± 6.9 µm	129.2 ± 2.3 µm
otpb:gfp	12	control MO	83.7 ± 5.4µm	129.1 ± 3.1 µm
Genotype	***n***	**Injection**	**Average distance of group 2 DA neurons toward the midline (left and right side combined**	**Average distance of group 4 DA neurons toward the midline (left and right side combined**
otpb:gfp	13	*sim1a + PM + UV*	32.1 ± 6.9 µm	36.5 ± 5.5 µm
otpb:gfp	12	control MO	33.2 ± 3.4 µm	34.1 ± 3.6 µm
Genotype	***n***	**Injection**	**Average distance between MA neurons**	
otpb:gfp	11	sim1a + PM + UV	123.6 ± 2.3 µm	
otpb:gfp	10	control MO	124.1 ± 2.2 µm	

To quantify the axon guidance effects in *sim1a* photomorph experiments, we measured the distance between longitudinal TH-positive axons at the anterior-posterior level of noradrenergic locus coeruleus (LC) neurons (Fig. 2B). To control for specificity of the observed effects, we determined the distance between the cell bodies of LC neurons (Fig. 2B) and of the MA neurons. In addition, we determined the distance of group 2 and 4 DA neurons from the midline (Fig. 2A). This analysis demonstrated a significant decrease of the distance between TH-positive longitudinal axons in *sim1a* photomorphants when compared with control MO-injected embryos. The distance between the LC neurons or MA neurons or positioning of DA neurons was not altered.

Absolute values with s.d. of average distances in µm are shown; *n* indicates number of embryos analyzed.

Table S6. Quantification of axon guidance defects in *robo2* mutant larvae (Fig. 3)

Genotype	***n***	**Average distance between longitudinal *otpb:gfp* axons at the level of the MA neurons**	**Average distance between longitudinal *hcrt:tdtomato* axons at the level of the MA neurons**	**Average distance between MA neurons**
ast^{ti272z}/+;*otpb:gfp*;*hcrt:tdtomato*	6	41.9± 5.4 µm	39.3± 5.4 µm	122.3± 3.5 µm
ast$^{ti272z/ti272z}$;*otpb:gfp*;*hcrt:tdtomato*	7	15.3± 2.7 µm	18.2± 5.3 µm	121.7± 2.5 µm

For quantification we determined the distance between *otpb:gfp* axons and *hcrt:tdtomato* axons at the level of the Mauthner neurons. To control for specificity, we determined the distance between MA neurons. This analysis demonstrated a significant decrease of the distance between *otpb:gfp* and *hcrt:tdtomato* longitudinal axons in *ast* mutants when compared with heterozygous *ast* controls. Distance between MA neurons was not different.

Absolute values with s.d. of average distances in µm are shown; *n* indicates number of embryos analyzed.

Table S7. Quantification of axon guidance defects in *robo3/twt* mutant larvae (Fig. 5 and Fig. S8)

Genotype	***n***	**Average distance between longitudinal *otpb:gfp* or *hcrt:tdtomato* axons at the level of the nucMLF neurons**	**Average distance between longitudinal *otpb:gfp* or *hcrt:tdtomato* axons at the level of the Mauthner neurons**
twt$^{tw204/+}$;*otpb:gfp*	21	182.9 ± 8.7 µm	64.8 ± 4.7 µm
twt$^{tw204/tw204}$;*otpb:gfp*	21	201.1 ± 10.8 µm	77.4 ± 6.2 µm
twt^{tw204}/+;*hcrt:tdtomato*	16	156.9 ± 9.4 µm	69.7 ± 7.8 µm
twt$^{tw204/tw204}$;*hcrt:tdtomato*	17	158.7 ± 9.4 µm	66.2 ± 7.6 µm

Genotype	***n***	**Average distance between nucMLF neurons in midbrain**	**Average distance between nucMLF axons at the level of MA neurons**
twt$^{tw204/+}$;*otpb:gfp*	21	77.9 ± 2.8 µm	14.6 ± 1.6 µm
twt$^{tw204/tw204}$;*otpb:gfp*	21	78.3 ± 2.4 µm	14.8 ± 1.6 µm
twt^{tw204}/+;*hcrt:tdtomato*	16	76.3 ± 3.6 µm	15.8 ± 1.8 µm
twt$^{tw204/tw204}$;*hcrt:tdtomato*	17	79.1 ± 3.6 µm	15.5 ± 1.6 µm

Genotype	***n***	**Average distance between MA neurons**
twt$^{tw204/+}$;*otpb:gfp*	21	123.2 ± 2.5 µm
twt$^{tw204/tw204}$;*otpb:gfp*	21	123.4 ± 3.8 µm
twt^{tw204}/+;*hcrt:tdtomato*	16	123.3 ± 3.2 µm
twt$^{tw204/tw204}$;*hcrt:tdtomato*	17	123.2± 3.3 µm

To analyze the role of *robo3* during HTS longitudinal axon guidance, the distance between *otpb:gfp* or *hcrt:tdtomato* longitudinal axons was determined at two different positions (see Fig. 5B). The first measurement was taken at the level of nucMLF neurons in the midbrain, shortly posterior to the level where *otpb:gfp*-positive axons have left the diencephalon. The second measurement was taken in the hindbrain at the level of the Mauthner neurons. To control for the specificity of the observed effects, we determined the distance between the nucMLF neurons and the distance between the nucMLF axons at the level of the Mauthner neurons (Fig. 5D,E). In addition, we determined the distance between the MA neurons. This analysis revealed a significant difference in the distance of longitudinal *otpb:gfp* axons in homozygous *twt* mutants when compared with heterozygous *twt* siblings. The distance between longitudinal *hcrt:tdtomato* axons, nucMLF neurons and their axons and the between the MA neurons was not different in either genotype (Fig.5E, Fig. S8H).

Absolute values with s.d. of average distances in µm are shown; *n* indicates number of embryos analyzed.

Table S8. Quantifications of axon tract position defects after *sim1a* or *arnt2* depletion experiments in *robo3/twt* mutant background (Fig. 5 and Fig. S9)

Genotype	***n***	**Injection**	**Average distance between *otpb:gfp* vagal nerve at ventral turning point**	**Average distance between *otpb:gfp* longitudinal axons at ventral turning point of potential vagal nerve**
twt$^{tw204/}$+;*otpb:gfp*	17	*sim1a* MO	141.5 ± 7.5 µm	22.3 ± 3.4 µm
twt$^{tw204/tw204}$;*otpb:gfp*	18	*sim1a* MO	144.5 ± 10.3 µm	47.1 ± 5.9 µm
twt$^{tw204/}$+;*otpb:gfp*	7	*arnt2* MO	142.4 ± 4.5 µm	27.7 ± 3.3 µm
twt$^{tw204/tw204}$;*otpb:gfp*	7	*arnt2* MO	144.8 ± 4.4 µm	49.9 ± 3.7 µm
Genotype	***n***	**Injection**	**Average distance between MA neurons**	**Average distance between *otpb:gfp* longitudinal axons at level of MA neurons**
twt$^{tw204/}$+;*otpb:gfp*	17	*sim1a* MO	122.1 ± 3.2 µm	21.9 ± 6.1
twt$^{tw204/tw204}$;*otpb:gfp*	18	*sim1a* MO	121.6 ± 3.4 µm	44.1 ± 7.6
twt$^{tw204/}$+;*otpb:gfp*	7	*arnt2* MO	122.2 ± 2.7 µm	37.8 ± 7.4
twt$^{tw204/tw204}$;*otpb:gfp*	7	*arnt2* MO	123.3 ± 2.7 µm	63.2 ± 8.2

In order to analyze the effect upon *sim1a* or *arnt2* depletion on longitudinal *otpb:gfp* axons in *twt* mutants, the distance between the bilateral *otpb:gfp*-positive longitudinal axon bundles was determined. To control for specificity, the distance between *otpb:gfp*-positive axons potentially derived from Xth (vagal) nerve neurons was determined. Both measurements were taken at an anterior-posterior level where the *otpb:gfp* positive potential vagal nerve axons turn ventrally (arrows in Fig. 5G). In addition, the distance between the MA neurons was determined. This analysis demonstrated a significant larger distance between *otpb:gfp* longitudinal axons in *twt* homozygous mutants after depletion of *sim1a* or *arnt2* when compared with heterozygous *twt* embryos. The distance between *otpb:gfp* vagal nerves or MA neurons was not different in either genotype (Fig. 5J and Fig. S9E).

Absolute values with s.d. of average distances in µm or average numbers are shown; *n* indicates number of embryos analyzed.

Table S9. Quantification of axon tract position defects after *sim1a* photomorph experiments in *robo3* mutant background (Fig. S10)

Genotype	***n***	**Injection**	**Average distance between LC neurons**	**Average distance between longitudinal TH positive axons at the level of the LC neurons**
twt$^{tw204/}$+	11	*sim1a* MO + PM	130.1 ± 9.8 µm	54,4 ± 8,4 µm
twt$^{tw204/tw204}$	12	*sim1a* MO + PM	131.2 ± 5.2 µm	84,3 ± 10,6 µm
Genotype	***n***	**Injection**	**Average distance between MA neurons**	
twt$^{tw204/+}$	7	*sim1a MO + PM*	121.5 ± 2.8 µm	
twt$^{tw204/tw204}$	7	*sim1a MO + PM*	123.3 ± 1.1 µm	

To analyze the effect upon *sim1a* photomorph experiment in *twt* mutants, we measured the distance between longitudinal TH-positive axons at the anterior-posterior level of noradrenergic LC neurons. Normal hindbrain development was confirmed by comparing the distance between the LC neurons, which was similar in *twt* heterozygous and mutant embryos. This analysis revealed a significant difference in the distance of TH-positive longitudinal axons in *twt* homozygous photomorphants when compared with heterozygous *twt* embryos. The distance of LC neurons or MA neurons was not different in either genotype (Fig. S10E).

Absolute values with s.d. of average distances in µm or average numbers are shown; *n* indicates number of embryos analyzed.

Table S10. Quantification of axon positions after overexpression of *robo3a.1* or *robo3b.1* in *otpb:gfp* background (Fig. 6A-G)

Genotype	*n*	Average number of *otpb:gfp* axons in inner segment	Average distance between MA neurons
otpb:gfp	16	0.9 ± 0.8	104.9 ± 4.1 µm
otpb:gfp; hsp70l:robo3a.1	16	2.9 ± 1.2	102.9 ± 6.5 µm
otpb:gfp, hsp70l:robo3b.1	16	0.7 ± 0.8	106.3 ± 6.0 µm

To quantify the effects after overexpression of *robo3a.1* or *robo3b.1*, we counted the number of longitudinal *otpb:gfp* longitudinal axons in an inner section, as defined by the distance between the MA neurons (Fig. 6B,B′,D,F). To control for specificity, we determined the distance of the MA neurons. This analysis revealed a significant increase in the number of longitudinal *otpb:gfp* axons in the inner section after overexpression of *robo3a.1* when compared with controls or after *robo3b.1* overexpression (Fig. 6A-G). This distance of the MA neurons was not different among the experimental groups.

Absolute values with s.d. of average distances in µm or average numbers are shown; *n* indicates number of embryos analyzed.

Table S11. Quantification of axon positions after overexpression of *robo3a.1* or *robo3b.1* in *hcrt:tdtomato* background (Fig. 6H-N)

Genotype	*n*	Average number of *hcrt:tdtomato* axons in outer segments	Average number of *hcrt:tdtomato* axon in inner segments	Average total number of *hcrt:tdtomato* axons	Average distance between MA neurons
hcrt:tdtomato	18	9.2 ± 1.5	0.6 ± 0.8	9.8 ± 1.5	131.1 ± 7.6 µm
hcrt:tdtomato; hsp70l:robo3a.1	19	6.1 ± 1.3	3.7 ± 0.7	9.8 ± 1.5	127.9 ± 6.9 µm
hcrt:tdtomato, hsp70l:robo3b.1	18	8.5 ± 0.9	0.7 ± 0.8	9.2 ± 1.2	127.2 ± 6.1 µm
Genotype		**Average distance of anterior Hcrt neurons toward the midline (left and right side combined)**			
hcrt:tdtomato	10	30.4 ± 3.1			
hcrt:tdtomato; hsp70l:robo3a.1	10	30.2 ± 2.3			
hcrt:tdtomato, hsp70l:robo3b.1	10	30.1 ± 3.4			

To quantify the effects after overexpression of *robo3a.1* or *robo3b.1*, we divided the hindbrain at the anterior-posterior level of the Mauthner neurons into an inner (medial) and two outer (lateral) sections (Fig. 6I), and counted the number of longitudinal *hcrt:tdtomato* axons in each section. To control for specificity, we determined the distance of the MA neurons and the distance of the most anterior Hcrt neurons. This analysis revealed a significant increase in the number of longitudinal *hcrt:tdtomato* axons in the inner section after overexpression of *robo3a.1* when compared with controls or after *robo3b.1* overexpression (Fig. 6F-H,M). This distance of the MA or Hcrt neurons was not different among the experimental groups.

Absolute values with s.d. of average distances in µm or average numbers are shown; *n* indicates number of embryos analyzed.

Table S12. Quantification axon positions after combined injections of *sim1a* and *dcc* in *otpbgfp* embryos (Fig. 7)

Genotype	*n*	Injection	Average distance between longitudinal *otpb:gfp* axons at the level of the Mauthner neurons	Average distance between Mauthner neurons
otpb:gfp	22	*sim1a* MO and control MO	27.9 ± 4.4 µm	116.9 ± 1.7 µm
otpb:gfp	23	*sim1a* MO and *dcc* MO	50.2 ± 8.1 µm	117.4 ± 1.3 µm

To analyze longitudinal *otpb:gfp* axon guidance after combined knock down of *sim1a* and *dcc*, we measured the average distance between the closest *otpb:gfp*-positive longitudinal axons at the level of the Mauthner neurons. This analysis revealed an increased distance of longitudinal axons upon depletion of *sim1a* and *dcc* when compared with controls. To control for specificity, we determined the distance between the MA neurons, which was not different (Fig. 7B,E).

Absolute values with standard deviations of average distances in µm or average numbers are shown;
n indicates number of embryos analyzed.

Table S13. Quantification of axon positions after injection of *sim1a* or control MO into *ast ;twt* compound mutants (Fig. 8)

Genotype	*n*	Injection	Distance between *otpb:gfp* vagal nerve at ventral turning point	Distance between *otpb:gfp* longitudinal axons at ventral turning point of potential vagal nerve
twt^{tw204}/+;*ast*$^{ti272z/ti272z}$ *otpb:gfp*	16	*sim1a* MO	129.4 ± 2.9 µm	15.2 ± 2.7 µm
twt$^{tw204/tw204}$;*ast*$^{ti272z/ti272z}$;*otpb:gfp*	16	*sim1a* MO	132.1 ± 3.7 µm	15.6 ± 2.3 µm
twt$^{tw204/tw204}$;*ast*$^{ti272z/ti272z}$;*otpb:gfp*	16	Control MO	128.1 ± 3.5 µm	15.6 ± 2.5 µm
Genotype	***n***	**Injection**	**Average distance between Mauthner neurons**	**Distance between *otpb:gfp* longitudinal axons at level of MA neurons**
twt^{tw204}/+;*ast*$^{ti272z/ti272z}$ *otpb:gfp*	16	*sim1a* MO	120.9 ± 2.3 µm	14.4 ± 1.9 µm
twt$^{tw204/tw204}$;*ast*$^{ti272z/ti272z}$;*otpb:gfp*	16	*sim1a* MO	120.8 ± 2.7 µm	16.5 ± 2.1 µm
twt$^{tw204/tw204}$;*ast*$^{ti272z/ti272z}$;*otpb:gfp*	16	Control MO	122.3 ± 2.5 µm	16.1 ± 2.3 µm

To determine medial displacement phenotype in *sim1a* or control MO-injected *ast;twt* compound mutant embryos, we measured the distances between *otpb:gfp* longitudinal axons and vagal axons. In addition, the distance between the MA neurons was determined. This analysis revealed no differences for the measurements.

Absolute values with standard deviations of average distances in µm or average numbers are shown;
n indicates number of embryos analyzed.

Table S14. Quantification of axon positions after overexpression of *robo3a.1* in weak and strong *ast* mutants (Fig. 9)

Genotype	***n***	**Average number of *hcrt:tdtomato* axons in outer segments**	**Average number of *hcrt:tdtomato* axon in inner segments**	**Average total number of *hcrt:tdtomato* axons**	**Average distance between MA neurons**
ast$^{ti272z/ti272z}$; hcrt:tdtomato	18	1.3 ± 1.4	8.7 ± 1.2	9.5 ± 2.6	130.1 ± 6.8 µm
ast$^{ti272z/ti272z}$; hcrt:tdtomato; hsp70l:robo3a.1	18	1.8 ± 1.5	7.2 ± 1.7	9.6 ± 1.6	129.1 ± 6.5 µm
ast$^{te284/te284}$; hcrt:tdtomato	17	4.7 ± 1.7	3.7 ± 1.6	8.4 ± 0.9	126.3 ± 3.8 µm
ast$^{te284/te284}$; hcrt:tdtomato; hsp70l:robo3a.1	17	1.3 ± 0.9	6.7 ± 1.0	8.1 ± 1.1	125.1 ± 4.5 µm
Genotype	***n***	**Average distance of anterior Hcrt neurons toward the midline (left and right side combined)**			
ast$^{ti272z/ti272z}$; hcrt:tdtomato	10	31.3 ± 2.6			
ast$^{ti272z/ti272z}$; hcrt:tdtomato; hsp70l:robo3a.1	10	30.9 ± 2.7			
ast$^{te284/te284}$; hcrt:tdtomato	10	29.9 ± 2.7			
ast$^{te284/te284}$; hcrt:tdtomato; hsp70l:robo3a.1	10	30.5 ± 2.6			

The effects upon overexpression of *robo3a.1* in the weak and strong *ast* mutant background were quantified by making use of the inner and outer sections (Fig. 9B,F,K,O) as described above for Fig. 6. This analysis revealed a significant increase in the number of longitudinal *hcrt:tdtomato* axons in the inner section after overexpression of *robo3a.1* in the weak *ast* mutants when compared with controls or the strong *ast* mutants (Fig. 9I,R). To control for specificity, we determined the distance of the MA neurons or the distance of the most anterior Hcrt neurons, which was not different.
Absolute values with s.d of average distances in µm or average numbers are shown; *n* indicates number of embryos analyzed.

Table S15. Quantification of MA neuron distance after overexpression of *robo3a.1*, *robo3b.1*, *Robo3A.1* and *Robo3A.2* using GAL4/UAS approach (Fig. 10)

Injection	***n***	**Average distance between MA neurons**
UAS:tdtomato	22	123.3 ± 3.5 µm
UAS:robo3a.1p2Atdtomato	23	123.3 ± 2.2 µm
UAS:robo3b.1p2Atdtomato	21	122.5 ± 2.9 µm
UAS:Robo3A.1p2Atdtomato	20	122.6 ± 4.4 µm
UAS:Robo3A.2p2Atdtomato	21	122.3 ± 4.7 µm
Injection	***n***	**Average distance between Hcrt neurons**
UAS:tdtomato	10	29.3 ± 3.3
UAS:robo3a.1p2Atdtomato	10	29.2 ± 3.7
UAS:robo3b.1p2Atdtomato	10	30.2 ± 4.2
UAS:Robo3A.1p2Atdtomato	10	30.4 ± 4.7
UAS:Robo3A.2p2Atdtomato	10	30.1 ± 3.6

To control for specificity upon mis-expression of the different *robo3* isoforms using a *hcrt:gal4* driver in combination with the UAS constructs mentioned below, we determined the distance of the MA and Hcrt neurons, which was not different.
Absolute values s.d. of average distances in µm or average numbers are shown; *n* indicates number of embryos analyzed.